

RESEARCH ARTICLE

In vivo Ca^{2+} dynamics in single pancreatic β cells

Stefan Jacob | Martin Köhler | Philip Tröster | Montse Visa |
 Concha F. García-Prieto | Tomas Alanentalo | Tilo Moede | Barbara Leibiger |
 Ingo B. Leibiger | Per-Olof Berggren

The Rolf Luft Research Center for Diabetes and Endocrinology, Karolinska Institutet, Stockholm, Sweden

Correspondence

Philip Tröster and Per-Olof Berggren, The Rolf Luft Research Center for Diabetes and Endocrinology, Karolinska University Hospital Solna L1:03, SE-171 76 Stockholm, Sweden.

Email: philip.troster@ki.se (P. T.) and Per-Olof.Berggren@ki.se (P.-O. B.)

Funding information

Svenska Forskningsrådet Formas (Swedish Research Council Formas); Erling-Persson Foundation; Stichting af Jochnick Foundation (Jochnick Foundation); Novo Nordisk Foundation Center for Basic Metabolic Research (NovoNordisk Foundation Center for Basic Metabolic Research); Swedish Diabetes Association; Scandia Insurance Company Ltd; Diabetes Research and Wellness Foundation; Berth von Kantzow's Foundation; Strategic Research Program in Diabetes at Karolinska Institutet; BetaImage, Grant/Award Number: ERC-2013-AdG 338936; BETASCREEN, Grant/Award Number: ERC-2017-PoC 727306; Swedish Foundation for Strategic Research; Knut och Alice Wallenbergs Stiftelse (Knut and Alice Wallenberg Foundation); EYELETS, Grant/Award Number: ERC-2018-AdG 834860

Abstract

The dynamics of cytoplasmic free Ca^{2+} concentration ($[\text{Ca}^{2+}]_i$) in pancreatic β cells is central to our understanding of β -cell physiology and pathology. In this context, there are numerous in vitro studies available but existing in vivo data are scarce. We now critically evaluate the anterior chamber of the eye as an in vivo, non-invasive, imaging site for measuring $[\text{Ca}^{2+}]_i$ dynamics longitudinally in three dimensions and at single-cell resolution. By applying a fluorescently labeled glucose analogue 2-(N-(7-Nitrobenz-2-oxa-1,3-diazol-4-yl)Amino)-2-Deoxyglucose in vivo, we followed how glucose almost simultaneously distributes to all cells within the islet volume, resulting in $[\text{Ca}^{2+}]_i$ changes. We found that almost all β cells in healthy mice responded to a glucose challenge, while in hyperinsulinemic, hyperglycemic mice about 80% of the β cells could not be further stimulated from fasting basal conditions. This finding indicates that our imaging modality can resolve functional heterogeneity within the β -cell population in terms of glucose responsiveness. Importantly, we demonstrate that glucose homeostasis is markedly affected using isoflurane compared to hypnorm/midazolam anesthetics, which has major implications for $[\text{Ca}^{2+}]_i$ measurements. In summary, this setup offers a powerful tool to further investigate in vivo pancreatic β -cell $[\text{Ca}^{2+}]_i$ response patterns at single-cell resolution in health and disease.

KEYWORDS

calcium dynamics, diabetes mellitus, fluorescence microscopy, in vivo imaging, pancreatic islets

Abbreviations: 2-NBDG, 2-(N-(7-Nitrobenz-2-oxa-1,3-diazol-4-yl)Amino)-2-Deoxyglucose; ACE, anterior chamber of the eye; EMCCD, electron multiplying charge-coupled device; HBSS, Hank's Balanced Salt Solution; Hyp/Mid, hypnorm/midazolam; IpGTT, intraperitoneal glucose tolerance test; IpITT, intraperitoneal insulin tolerance test; $[\text{Ca}^{2+}]_i$, intracellular free calcium ion concentration; RIP, rat insulin promoter.

Stefan Jacob, Martin Köhler, and Philip Tröster contributed equally to the presented work.

This is an open access article under the terms of the Creative Commons Attribution-NonCommercial License, which permits use, distribution and reproduction in any medium, provided the original work is properly cited and is not used for commercial purposes.

© 2019 The Authors. The FASEB Journal published by Wiley Periodicals, Inc. on behalf of Federation of American Societies for Experimental Biology

1 | INTRODUCTION

Pancreatic islets play a primary role in the control of glucose homeostasis. In response to elevated blood glucose concentrations, pancreatic β cells secrete insulin by Ca^{2+} -triggered exocytosis.^{1,2} In this context, Ca^{2+} signaling has been extensively used as a readout for β -cell function under physiological and pathological conditions.³ A β -cell dysfunction in combination with peripheral insulin resistance is central to the development of type 2 diabetes, a still growing pandemic disease leading to hyperglycemia. To understand the development of diabetes, it is of great importance to reveal how the pancreatic β -cell network operates at single-cell level while integrating a variety of signals in response to changing metabolic demands under physiological conditions. Previous measurements of β -cell cytoplasmic free Ca^{2+} concentration ($[\text{Ca}^{2+}]_i$) have implied that the β -cell network consists of subpopulations which demonstrate functional heterogeneity during glucose stimulation.⁴⁻⁶ Although these findings provide important insights into β -cell function, the results are exclusively based either on ex vivo or in vitro data and disregard important factors provided by blood supply, innervation, as well as the metabolic state of islet/ β cells under in vivo conditions.

The present study analyzes β -cell $[\text{Ca}^{2+}]_i$ dynamics of mouse islets in the living organism by transplanting GCaMP3-expressing sensor islets into the anterior chamber of the eye (ACE). Admittedly, the eye-transplantation site does not entirely represent the in situ situation, which could, for example, result from lack of endocrine-exocrine communication. However, prior experiments indicate that the function of β cells in the eye is mainly comparable to their function in situ. Our previous studies demonstrated that intraocular islets engraft onto the iris of recipient animals by developing full vascularization and innervation after 4 weeks.^{7,8} The transplanted islets are metabolically active and capable of controlling blood glucose levels.⁸ Although a non-invasive in vivo imaging technique of intraocular islets has already been used to measure Ca^{2+} dynamics in β cells,⁹ the approach has not been demonstrated at single-cell resolution. In the following, we describe how we advanced our in vivo imaging technique using additional image processing which allows us to analyze single β -cell $[\text{Ca}^{2+}]_i$ dynamics within an islet volume during the response to glucose stimulation. In addition, we could show that the glucose response of an eye-engrafted islet has only a short latency of around 12 seconds after intravenous glucose injection. Moreover, we could demonstrate that the choice of an appropriate anesthetic agent is crucial for the in vivo imaging to avoid impact on glucose metabolism and Ca^{2+} signaling. Acknowledging the overall strength of the ACE for in vivo imaging, there is an immediate need to specifically adjust experimental data for unwanted side effects associated with the procedure itself, for example, the

proper use of anesthetics when studying $[\text{Ca}^{2+}]_i$ dynamics. Finally, we proved that intraocular sensor islets can adapt to the metabolic milieu of their host animal by showing modified β -cell $[\text{Ca}^{2+}]_i$ patterns. In young leptin-deficient mice suffering from hyperinsulinemia and hyperglycemia, only about 20% of the β cells could be stimulated by an additional glucose challenge, indicating that a functional heterogeneity regarding glucose responsiveness was present in the glucose-sensing β cells of the intraocular-transplanted islets.

2 | MATERIALS AND METHODS

2.1 | Mice

Sensor islets were isolated from double heterozygous donor animals (RIP-Cre:GCaMP3), which were obtained by crossing the RIP-Cre mouse line (B6.Cg-*Tg(Ins2-cre)25Mgn/J*) with the Ai38 floxed GCaMP3 reporter mouse line (B6;129S-*Gt(ROSA)26Sor^{tm38(CAG-GCaMP3)Hze/J}*) (both purchased from The Jackson Laboratories (Bar Harbor, ME)). Congenic Ob (Lep^{ob}/Lep^{ob}) and Lean (Lep⁺/Lep⁺) mice, backcrossed into C57BL/6J genetic background, were obtained from our breeding colony at Karolinska Institutet, Stockholm, Sweden. The use of animals was approved by the Swedish Animal Council and complied with the "Guide for the care and use of laboratory animals," Eighth edition (2011).

2.2 | Islet isolation and transplantation

Islets were isolated from either wild-type or double heterozygous RIP-Cre:GCaMP3 mice, which were backcrossed with a C57BL/6J mouse line for more than 10 generations. Donor animals were sacrificed and 2.5 mL ice cold Collagenase A (1.5 mg/mL) in Hank's Balanced Salt Solution (HBSS) supplemented with 0.2% (w/v) BSA in HEPES (pH 7.4) was injected into the pancreas via the cannulated common bile duct. The distended pancreas was transferred to a vial, filled with ice cold HBSS, and digested at 37°C for 25 minutes. After two gentle washing steps, islets were handpicked and incubated overnight in RPMI-1640 Medium (ThermoFisher Scientific, USA) supplemented with 10% (v/v) FBS, 2 mmol/L L-Glutamine (ThermoFisher Scientific, USA), 100 IU/mL penicillin (SigmaAldrich, USA), and 100 $\mu\text{g}/\text{mL}$ streptomycin (SigmaAldrich, USA). Using the UNIVENTOR 400 Anaesthesia Unit, recipient animals were constantly anesthetized with isoflurane (Baxter, USA) and fixated in a head holder (Narishige, Japan) in preparation for the islet transplantation.¹⁰ The cornea was punctured with a 27-gauge needle and a pulled glass micropipette (1.5 mm outer diameter, World Precision Instruments, USA), containing the islets, was inserted into the ACE. Five to six islets were injected

into the ACE and positioned on the iris around the pupil. Imaging was performed 4 weeks after transplantation in the Young Lean, Young Ob, and Old Ob animal group. Data of the Old Lean control group were obtained from seven animals imaged 4 weeks after transplantation and six animals imaged 6 weeks after transplantation. No differences between the two time points were detectable and the data of both are merged in the analysis.

2.3 | Glucose and insulin tolerance test

Glucose tolerance tests were performed by intraperitoneal glucose injection (2 g/kg body weight) after 6 hours of fasting in non-anesthetized control or anesthetized mice. Mice anesthetized either with a mixture of fentanyl (0.6 mg/kg), fluanisone (20 mg/kg), and midazolam (10 mg/kg) or with isoflurane (2%) inhalation were placed on a heating pad (37°C) under a heating lamp to simulate the warm environment within the microscope chamber. Oxygen was supplied through a nose mask at 250 mL/min. Tail blood glucose was measured prior to anesthesia and after mice were anesthetized at 0, 15, 30, 60, 90, and 120 minutes after glucose injection using a glucometer (Accu-Chek Aviva; F. Hoffmann-La Roche, Basel, Switzerland). Plasma insulin levels were measured in centrifuged blood samples taken at 0, 15, 30, and 60 minutes after glucose injection using an AlphaLISA immunoassay kit (Perkin Elmer, Waltham, MA) following manufacturer's instructions. For the intraperitoneal insulin tolerance test (IpITT), 0.5 U/kg human insulin (Novo Nordisk, Clayton, NC, USA) was injected intraperitoneally after 6 hours of fasting. Tail blood glucose was measured prior to anesthesia and after mice were anesthetized at 0, 15, 30, 60, 90, 120, and 180 minutes. Non-anesthetized mice were used as control mice.

2.4 | In vivo Ca^{2+} imaging of ACE-transplanted islets of Langerhans

Recipient mice were fasted for 4 hours, anesthetized either by intraperitoneal injection of fentanyl/fluanison/midazolam (0.6/20/10 mg/kg) or inhalation of 2% isoflurane and kept under a heat lamp. Mice were placed onto a heating pad with head fixation and oxygen supply (250 mL/min). 25 minutes after anesthesia induction, the eye was clamped and a tail vein catheter inserted. Heparin (14 μL , 100 IE/mL) in sterile saline was directly injected, while the rest of the catheter contained 20% (w/v) D-glucose in sterile saline separated by a small air bubble. Mice were placed under the microscope in a heated microscope chamber (37°C) and a pea-sized drop of pre-warmed ViscoTears (Thea Pharmaceuticals Limited, UK) was applied between eye and immersion objective. Intravenous D-glucose infusion (0.4 g/kg) was carefully

conducted 4 minutes after start of recording. Fluorescence imaging was performed with a Leica DM6000 CFS equipped with 25 \times /0.95 NA lens (Leica Microsystems, Germany; excitation: \sim 480 nm; emission: $>$ 500 nm). The whole microscope was enclosed to allow heating to 35°C. Fluorescence was collected by an electron multiplying charge-coupled device (EMCCD) (9100-13B or 9100-23B, Hamamatsu, Japan), while the objective was moved up and down by a piezoelectric actuator (NV 40/1 CLE, Piezosystem Jena, Germany) with an amplitude of 120 μm and a frequency of 0.5 Hz. The focus step size between single images was 4 μm . Objective motion and camera readout were synchronized by LabVIEW and NI-DAQ (National Instruments, USA). Images were acquired with HCIImage (Hamamatsu, Japan). Only one islet per animal was imaged during an experiment.

2.5 | Image processing and data analysis

Image processing was performed in MATLAB (MathWorks, USA) and every z -stack recording was first denoised.¹¹ The denoising procedure was based on estimation of the SURE threshold and consecutive wavelet filtering (4 scales). Consecutive planes within a z -stack were aligned within the imaging plane (translation only) using a method similar to cross correlation of the Fast Fourier Transform.¹² This method makes use of the large extension of the epifluorescence point spread function along the optical axes. Minor parts of eye motion occurring along the optical axes cannot be corrected and were present in the final z -stack. Z -stack recordings were deconvolved using a theoretically obtained point spread function, which was adjusted to the experimental conditions and was primarily meant to increase the contrast along the optical axis.¹³ In addition, every z -stack was registered in terms of translation and rotation to a reference z -stack.¹⁴ Fluorescence intensity gradients were used to compute translation and rotation parameters to make the registration more robust to the time-varying GCaMP3 fluorescence. Finally, single cells were selected by hand in 3D reconstruction and the average of all voxels belonging to a cell is presented as single cell $[\text{Ca}^{2+}]_i$ traces. Voxels belonging to a cell needed to have a correlation coefficient larger than 0.9 over the whole recording and needed to be within 20 μm in every spatial dimension. All single cells that could be identified in the imaged z -stack were selected and the islet average time trace was computed as an average over the time traces of all individual cells.

2.6 | 2-NBDG imaging

Islets from C57BL/6J donor mice were transplanted into the ACE of C57BL/6J mice. 2-(*N*-(7-Nitrobenz-2-oxa-1,3-diazol-4-yl)Amino)-2-Deoxyglucose (2-NBDG)

imaging was performed 4 weeks after transplantation to guarantee a fully developed vascularization of the transplant. The transplanted islets in anesthetized recipient mice were recorded with a confocal microscope (SP5 II on DM6000 CFS, Leica Microsystems, Germany; excitation: 488 and 633 nm, emission: 500-600 nm and 630-636 nm) by acquiring *z*-stacks every second. During the recording, 50 μ L of 5 mg/mL 2-NBDG (ThermoFisher Scientific, USA) dissolved in PBS (+/+) was injected via tail vein catheter. Image deconvolution was omitted from image processing. The second (633 nm) light channel, showing the backscatter reflection, was used to identify the three-dimensional boundaries of the islet. The bright 2-NBDG labeling of intra islet vasculature was used to define the location of the blood vessels within the islet. Interstitial space location was identified by spatial automatic peak detection of 2-NBDG fluorescence, with minimum prominence of 5 and peak width between 3 and 20 pixels for every time point. The interstitial space 2-NBDG intensity was then monitored as the prominence value.

2.7 | Statistical analysis

Data processing and statistical analysis were performed using Prism (version 7, GraphPad). Data are presented as mean \pm SEM. The *n*-numbers are indicated in the figure legends. Mann-Whitney *U* tests or two-way ANOVA followed by Tukey's post-hoc test were used, as appropriate. *P* values $<.05$ were considered statistically significant.

3 | RESULTS

3.1 | Imaging setup for single β -cell $[Ca^{2+}]_i$ dynamics analysis in vivo

$[Ca^{2+}]_i$ dynamics have been extensively used as a readout of β -cell functionality.¹⁵ However, few studies have been performed in vivo and most of them fail to achieve adequate single-cell resolution.⁹ We established a new in vivo imaging acquisition methodology using image analysis software to analyze $[Ca^{2+}]_i$ dynamics at single-cell resolution in islets transplanted into the ACE. For this purpose, we transplanted islets expressing the Ca^{2+} biosensor GCaMP3 exclusively in pancreatic β cells (RIP-Cre:GCaMP3) into the ACE of female recipient mice. Using the eye as a transplantation site, non-invasive intravital microscopy is possible, since the cornea is used as a natural body window for imaging. Engrafted islets were imaged in anesthetized animals 4 weeks after transplantation when islets were fully vascularized and innervated.

To obtain high temporal resolution images, we set up an imaging methodology based on epifluorescence microscopy. Three-dimensional images of transplanted islets were acquired by moving the objective in the axial direction by a piezoelectric actuator with the frequency of 0.5 Hz. Thereby, the upper 120- μ m hemisphere was acquired in 30 steps with 4 μ m intervals. Since the volume is imaged both during downward and upward motion, the 0.5 Hz frequency leads to a 1 Hz acquisition rate of the acquired volume. Objective movement and camera readout were externally synchronized by LabVIEW and NI-DAQ. A schematic

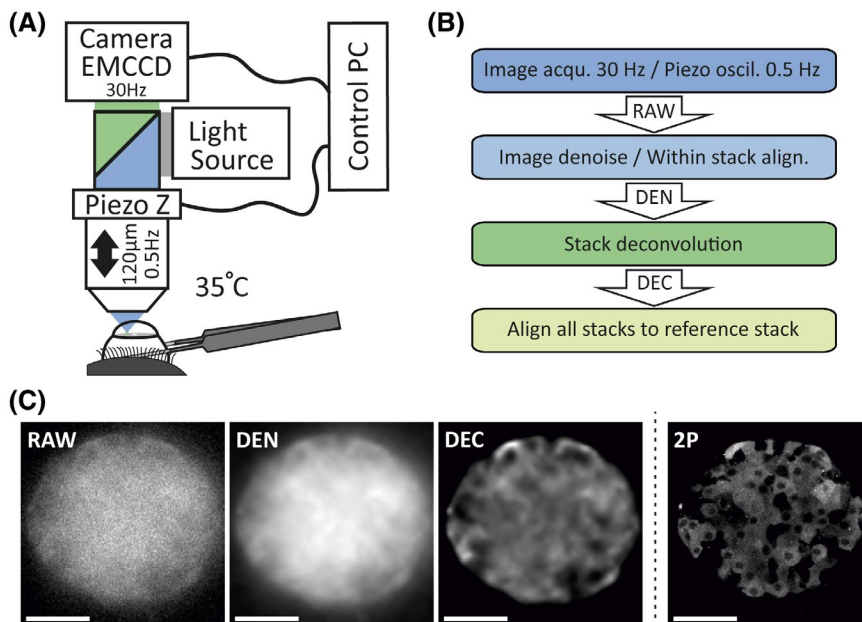


FIGURE 1 Three-dimensional image acquisition and post-processing of in vivo $[Ca^{2+}]_i$ recording in intraocular-transplanted islets. A, Schematic diagram of the microscope setup and (B) the consecutive image processing steps. C, 2D image sections of an intraocular-transplanted GCaMP3-expressing pancreatic islet illustrate the image enhancement during image processing. Raw image volumes (RAW) are denoised (DEN) and thereafter deconvolved (DEC). A two-photon image of the same islet is shown as comparison (2P); scale bar denotes 50 μ m

representation of the microscope setup is shown in Figure 1A. Unprocessed images obtained from the described imaging setup showed a significant noise level due to limited number of photons (Figure 1C, RAW). Therefore, further image processing using MATLAB was required to make single-cell analysis feasible, as outlined by the steps specified in Figure 1B. After denoising raw images, consecutive planes of z -stack images were aligned within the image plane due to movements during the experiment (Figure 1C, DEN). We further processed those images by deconvolution to increase image contrast along the optical axis. Images obtained through this process (Figure 1C, DEC) reached an image resolution that permits identification of single cells as illustrated here by an image of the same focal plane using multiphoton microscopy (Figures 1C, and 2P).

Before recording glucose-evoked β -cell $[Ca^{2+}]_i$ dynamics in vivo, recipient animals were fasted for 4 hours to obtain basal blood glucose levels in all experimental animals. Then individual transplanted RIP-Cre:GCaMP3 islets were imaged in their basal state for 4 minutes before the recipient animals were challenged with glucose stimulation via tail vein injection. The fluorescence intensity of GCaMP3 was recorded for another 20 minutes. Denoised and deconvolved image series were used to manually select individual cells in a specific z -plane as recognized by their GCaMP3 fluorescence (Figure 2A). About 50–200 β cells could be manually identified per islet. Figure 2B illustrates a representative $[Ca^{2+}]_i$ recording of an individual islet with varicolored fluorescence traces for every single β cell and a vertical red line indicating the glucose injection time point. In this recording, individual β cells displayed a similar fluorescence pattern over the entire recording period. In the basal state, the β -cell population revealed fast but faint $[Ca^{2+}]_i$ oscillations, which were interrupted by one extensive $[Ca^{2+}]_i$ peak after glucose injection.

The majority of β cells responded to glucose in a coordinated fashion, with time lags detectable between responding cells. The subsequent $[Ca^{2+}]_i$ dynamics differed from animal to animal often showing a combination of fast and slow $[Ca^{2+}]_i$ oscillations. The fluorescence intensities from all individual β cells were used to average the total β -cell $[Ca^{2+}]_i$ dynamics from one islet (Figure 2C). The overall $[Ca^{2+}]_i$ profile of individual fluorescence intensities clearly highlighted the time point when single β cells peaked in a synchronized way, which can even be represented in more detail by a heat map (Figure 2D).

3.2 | Dynamics of the glucose exposure in intraocular-transplanted islets

Two important factors affecting the β -cell $[Ca^{2+}]_i$ response to glucose stimulation in vivo are the vascular distribution and cellular uptake of glucose. To study how glucose reaches the β -cell population in our in vivo islet transplantation model, we

transplanted C57BL/6J mouse islets into the ACE of leptin-deficient mice $Lep^{ob/ob}$ (Ob) and their respective control littermates $Lep^{+/+}$ mice (Lean). The comparison between Ob and Lean animals is of importance in this study, since the type 2 diabetic mouse model is reported to have an abnormal blood vessel morphology.¹⁶ Altered glucose exposure to the β -cell network caused by vascular malformation have to be considered as an influential parameter in measurements of the β -cell $[Ca^{2+}]_i$ response patterns. Four weeks after transplantation, the sensor islets in the ACE were imaged during the course of iv administration of the fluorescent glucose analogue 2-NBDG. The interstitial fluid surrounding all islet cells was uniformly labeled by 2-NBDG about 3 seconds after the first fluorescence signal was detected in the islet vasculature. Representative time course images of 2-NBDG reaching the islet vasculature are shown in Figure 3A. Detailed analysis of the fluorescence intensity time course in control animals revealed that even regions more distant to the vasculature (20 μ m) showed almost the same onset time as regions in closer proximity to the blood vessels (10 μ m) (Figure 3B, Lean). These results suggest that iv injected glucose reaches all β cells within a vascularized islet at a similar time, which is in contrast to in vitro models, where the exposure of β cells to glucose depends on much slower and unbalanced diffusion.¹⁷ The same fast permeation into the interstitial space was observed in $Lep^{ob/ob}$ mice showing similar 2-NBDG fluorescence profiles compared to Lean control mice (Figure 3B, Ob). These data indicate that glucose transport from blood vessels to β cells is not impaired in $Lep^{ob/ob}$ mice.

Since the β cells in vivo are exposed to glucose almost at the same time, our experimental setting is well suited to measure the time it takes for β cells to respond to glucose with regard to $[Ca^{2+}]_i$. RIPCre:GCaMP3 expressing islets were transplanted into the ACE of C57BL6/J mice and imaged for β -cell $[Ca^{2+}]_i$ dynamics 4 weeks after transplantation. Glucose was injected into the tail vein together with Alexa 647-conjugated 10 kDa dextran to precisely determine the time point when glucose reaches the islet vasculature. This allowed us to measure the time interval between glucose arrival and the first Ca^{2+} response, defined as half maximum of relative increase in GCaMP3 fluorescence (Figure 3C). The delta time quantifications from several experiments showed that β cells are responding with $[Ca^{2+}]_i$ increase about 12 seconds after glucose reaches the islet (Figure 3D). To demonstrate that the dynamics of the glucose-stimulated $[Ca^{2+}]_i$ response within the β -cell network differs between the vascularized in vivo and the non-vascularized in vitro situation, we measured the initial $[Ca^{2+}]_i$ peak response in a perfusion chamber where the glucose propagation depends only on diffusion. The spread of the initial $[Ca^{2+}]_i$ response in vitro clearly shows a time delay which increases from the outer layer toward the center of the islet and which is in contrast to the rapid ubiquitous spread observed in vivo (Figure S1).

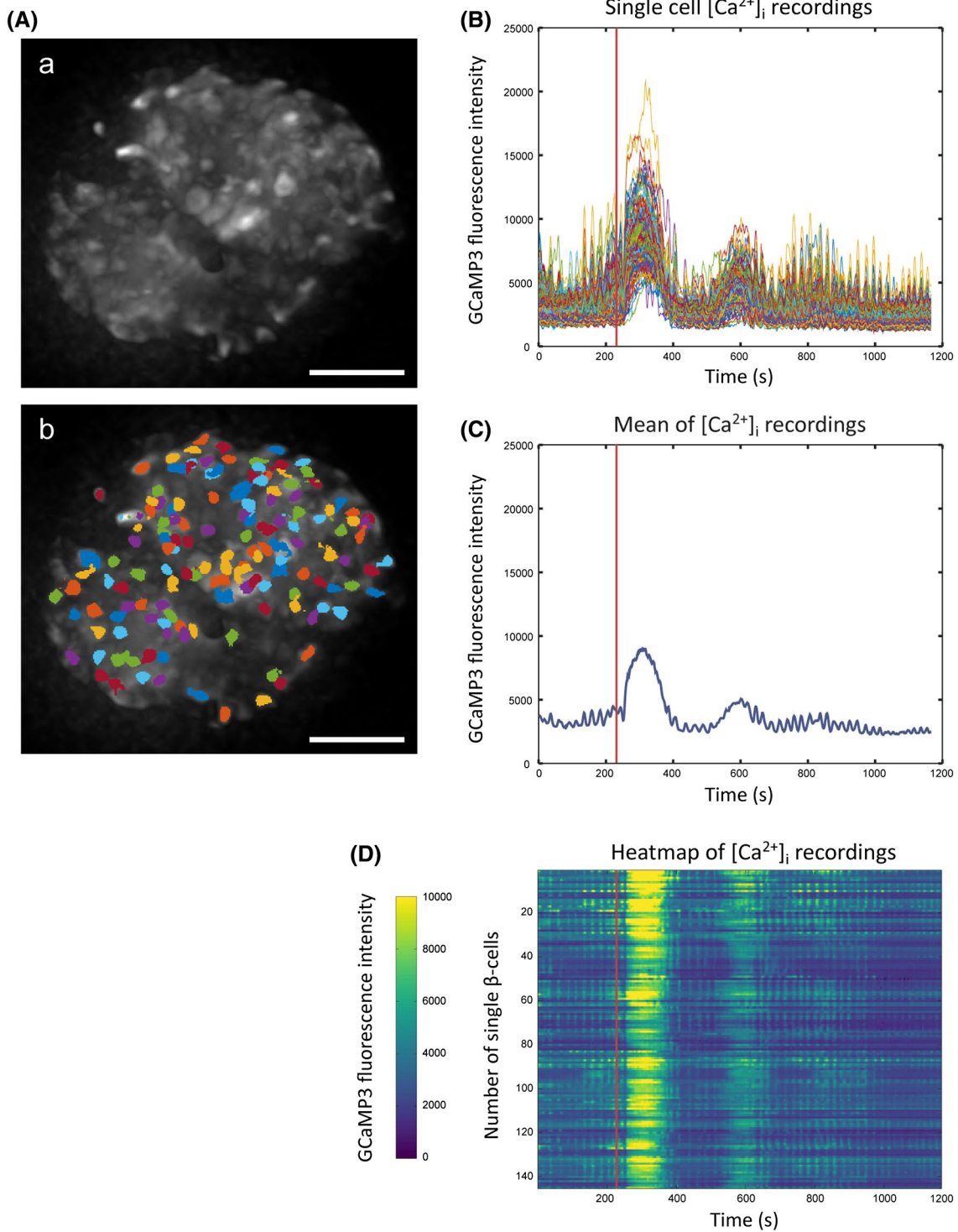


FIGURE 2 Illustration of single β -cell $[Ca^{2+}]_i$ dynamics in response to glucose stimulation. Aa, The maximum intensity projection of an intraocular-transplanted pancreatic RIP-Cre:GCaMP3 islet. Ab, The colored overlay illustrates the manual selection of regions of interest and the areas from which single β -cell data were obtained. B, The representation of fluorescence over time displays all individual β -cell $[Ca^{2+}]_i$ traces for one transplanted GCaMP3-expressing islet during the response to glucose stimulation. Time point of intravenous glucose injection is indicated by the red line. C, The average of all single β -cell $[Ca^{2+}]_i$ fluorescence intensities shows the islet $[Ca^{2+}]_i$ response in total. D, The heat map provides a clearer and more accessible representation of the individual β -cell $[Ca^{2+}]_i$ dynamics; color code denotes absolute fluorescence intensity

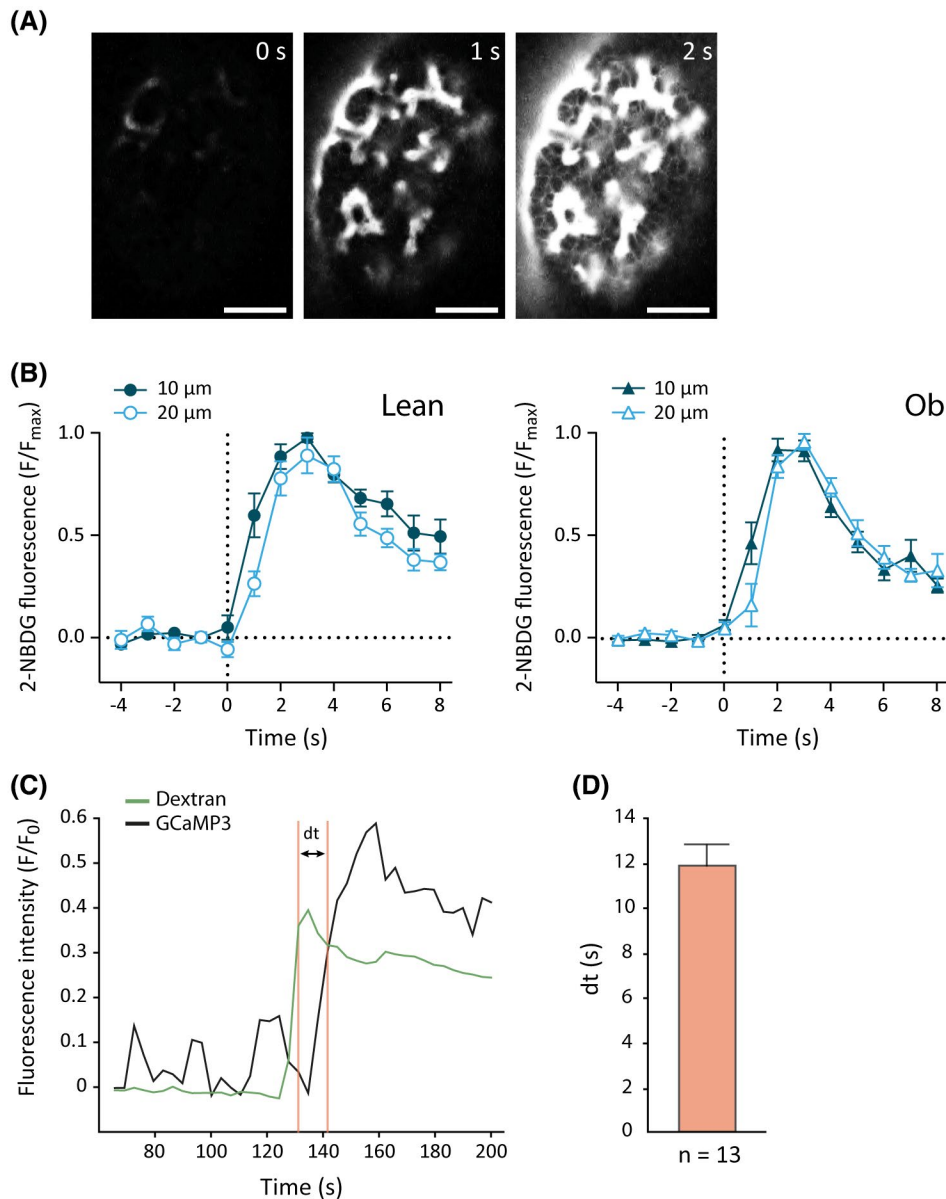


FIGURE 3 In vivo dynamics of β -cell exposure to glucose estimated by intravenous injection of 2-NBDG and onset time of β -cell $[Ca^{2+}]_i$ response. A, The confocal image sequence shows the first two seconds after intravenously injected 2-NBDG reaches the vasculature of an intraocular engrafted islet; scale bar denotes 50 μ m. B, Time courses of interstitial space labeling using 2-NBDG as fluorescent glucose analog. Islets were transplanted into either Lean ($n = 4$) or Ob ($n = 6$) animals. The diagrams show the time course of fluorescence intensity of 2-NBDG from the interstitial space within a distance of 10 and 20 μ m from the most proximal blood vessel within the vascularized islet; results are maximum (peak-basal) normalized and shown as means \pm SEM. C, In vivo recording of a RIP-Cre:GCaMP3 sensor islet transplanted in a C57BL/6J recipient displays the time correlation between glucose exposure in the vasculature and the glucose-stimulated $[Ca^{2+}]_i$ response in β cells. Alexa 647-conjugated dextran (10 kDa) was co-injected with the glucose challenge intravenously. The delta time (dt) between both fluorescence signals was determined by the time interval between the first Alexa 647 peak and the half maximum of stimulated GCaMP3 fluorescence. D, Delta time measurements ($n = 13$) reveal that β cells require about 12 seconds on average to actuate the $[Ca^{2+}]_i$ response after glucose has reached the blood vessel

3.3 | Anesthesia affects glucose metabolism and β -cell $[Ca^{2+}]_i$ dynamics

In vivo monitoring of β -cell $[Ca^{2+}]_i$ dynamics requires the anesthesia of mice during the imaging session. In this context, it is fundamental to determine whether and how anesthesia

influences the glucose homeostasis and consequently Ca^{2+} handling. To investigate the impact of anesthetics on insulin secretion and glucose homeostasis, we performed a glucose tolerance test (GTT) by intraperitoneal injection of glucose to conscious mice (Control) and mice anesthetized with either hypnorm/midazolam (Hyp/Mid) or isoflurane. Blood glucose

and insulin levels were measured at various time points. No significant differences in blood glucose levels were observed at time point 0, prior to glucose stimulation, when the animals were already under anesthesia by Hyp/Mid. However, isoflurane-anesthetized mice exhibited a noticeable increase in basal blood glucose level (comparison between time: - 15 minutes and 0) prior to glucose stimulation compared with control and Hyp/Mid groups. After the glucose challenge, no impaired glucose tolerance was observed for the Hyp/Mid group compared to the control group, whereas mice anesthetized with isoflurane demonstrated significant impaired glucose tolerance with high plasma glucose levels at minutes 60, 90, and 120 after glucose injection (Figure 4A). The area under the curve illustrates the significantly higher blood glucose level in mice anesthetized with isoflurane during the GTT (Figure 4B). Plasma insulin levels measured during GTT revealed that the glucose injection cannot induce insulin secretion in mice anesthetized with isoflurane (Figure 4C). This lack of insulin secretion explains the maintained high glucose levels observed during the GTT, suggesting that isoflurane severely disrupts glucose-induced insulin secretion. In contrast, mice from the Hyp/Mid group exhibited higher plasma insulin levels at all time points after glucose injection compared to the control mice with a similar insulin secretion profile (Figure 4C), indicating that mice under Hyp/Mid anesthesia are able to restore normoglycemia after glucose injection to the same degree as control mice but at the expense of increased insulin secretion. Therefore, we performed an IpITT to investigate whether the peripheral insulin sensitivity is affected by Hyp/Mid anesthesia (Figure 4F). The IpITT of both anesthesia groups reveals an increased glucose disposal in response to the insulin injection showing no evidence for an induced insulin resistance. While the blood sugar level of isoflurane anesthetized animals is impaired by acute hyperglycemia, the glucose homeostasis, and insulin sensitivity under the influence of Hyp/Mid anesthesia is in accordance with the conscious control animals.

Since Hyp/Mid anesthesia was applied in our *in vivo* Ca^{2+} imaging, we assessed *in vitro* whether this anesthetic agent has direct impact on the β -cell function. The insulin secretion of pancreatic β cells was examined by a perfusion system. In all, 50 isolated islets were exposed to perfusion medium with 3 mM glucose, 16.7 mM glucose, or 25 mM KCl supplemented with additional concentrations of Hyp/Mid and the amount of insulin in the perfusate per minute was determined (Figure S2A). It shows that a dose similar to that used in the *in vivo* imaging setup has no effect on the insulin secretory capacity of β cells. However, the same experiment with double doses of the Hyp/Mid anesthetic resulted in a slightly reduced amounts of insulin measured. In addition, to prove whether the Ca^{2+} handling of β cells is impaired by Hyp/Mid, we measured the initial $[\text{Ca}^{2+}]_i$ response peak after glucose stimulation *in vitro* using the higher doses of the Hyp/Mid anesthetic (Figure

S2B). It shows that the magnitude of the Ca^{2+} response in β cells is not altered in isolated islets under the influence of Hyp/Mid.

To study the impact of anesthetics on β -cell $[\text{Ca}^{2+}]_i$ dynamics, we transplanted islets expressing the Ca^{2+} biosensor GCaMP3 into the ACE of C57BL6/J mice. Four weeks after transplantation, the islets were imaged in mice that were either under Hyp/Mid or isoflurane anesthesia. We observed that mice under Hyp/Mid anesthesia exhibited a clear increase in $[\text{Ca}^{2+}]_i$ after glucose stimulation, which was progressively reduced over time until reaching β -cell $[\text{Ca}^{2+}]_i$ dynamics similar to the non-stimulated state before glucose injection (Figure 4D). These $[\text{Ca}^{2+}]_i$ dynamics of Hyp/Mid animals correlated with the blood glucose levels observed in the GTT. However, while $[\text{Ca}^{2+}]_i$ dynamics in β cells of mice anesthetized with isoflurane were also increased after glucose injection, the subsequent $[\text{Ca}^{2+}]_i$ profile completely differed from the Hyp/Mid mice group, showing a slowly oscillating $[\text{Ca}^{2+}]_i$ that was maintained during the subsequent recording (Figure 4E). These persistent $[\text{Ca}^{2+}]_i$ oscillations can be explained by the sustained high blood glucose level observed in the GTT, which constantly stimulates the β -cell glucose sensor and thereby induces the elevation in $[\text{Ca}^{2+}]_i$. However, the lack of insulin secretion after glucose injection observed during the GTT in mice anesthetized with isoflurane indicates that the observed $[\text{Ca}^{2+}]_i$ oscillations are not correlating with insulin secretion events anymore. β -cell $[\text{Ca}^{2+}]_i$ dynamics under normal conditions are closely associated with a permissive step for insulin secretion. Hence, our findings suggest that isoflurane anesthetic causes impaired glucose homeostasis and β -cell $[\text{Ca}^{2+}]_i$ dynamics which are then uncoupled from insulin exocytosis. Hyp/Mid anesthetic, on the other hand, seems to be suitable for the analysis of *in vivo* β -cell $[\text{Ca}^{2+}]_i$ dynamics showing minor impact on β -cell physiology.

3.4 | Sensor islets reveal altered β -cell $[\text{Ca}^{2+}]_i$ dynamics in young leptin-deficient mice

We next wanted to investigate how sensor islets can reflect physiological alterations in different animal models. For this purpose, we used a type 2 diabetic mouse model, the leptin-deficient $\text{Lep}^{\text{ob/ob}}$ mouse, which exhibits hyperinsulinemia and hyperglycemia at maximum levels between 3 and 5 months of age and a progressively decreasing glycemia until becoming normoglycemic at approximately 12 months of age. We transplanted sensor islets expressing GCaMP3 into the ACE of 3-5 or 10-months-old $\text{Lep}^{\text{ob/ob}}$ mice (Young Ob or Old Ob, respectively) and their respective age-matched wild-type $\text{Lep}^{+/+}$ control animals (Young Lean or Old Lean). β -cell $[\text{Ca}^{2+}]_i$ dynamics in response to glucose stimulation was evaluated 4 weeks after transplantation. Representative

β -cell $[Ca^{2+}]_i$ fluorescence intensity traces for every experimental group were averaged from single β -cell assessments and shown per islet (Figure 5A). After glucose injection into the tail vein of recipient animals (injection time point is indicated by the red vertical line), an initial peak in the β -cell $[Ca^{2+}]_i$ profile is followed by diversified $[Ca^{2+}]_i$ oscillations.

The $[Ca^{2+}]_i$ dynamics of both 10-months-old groups, Old Lean and Old Ob, reveal to be similar in the initial peak after glucose challenge and the following regular $[Ca^{2+}]_i$ oscillations. However, the $[Ca^{2+}]_i$ traces of the two younger animal groups deviated from this. While the Young Lean animals still showed, albeit a slightly diminished initial peak,

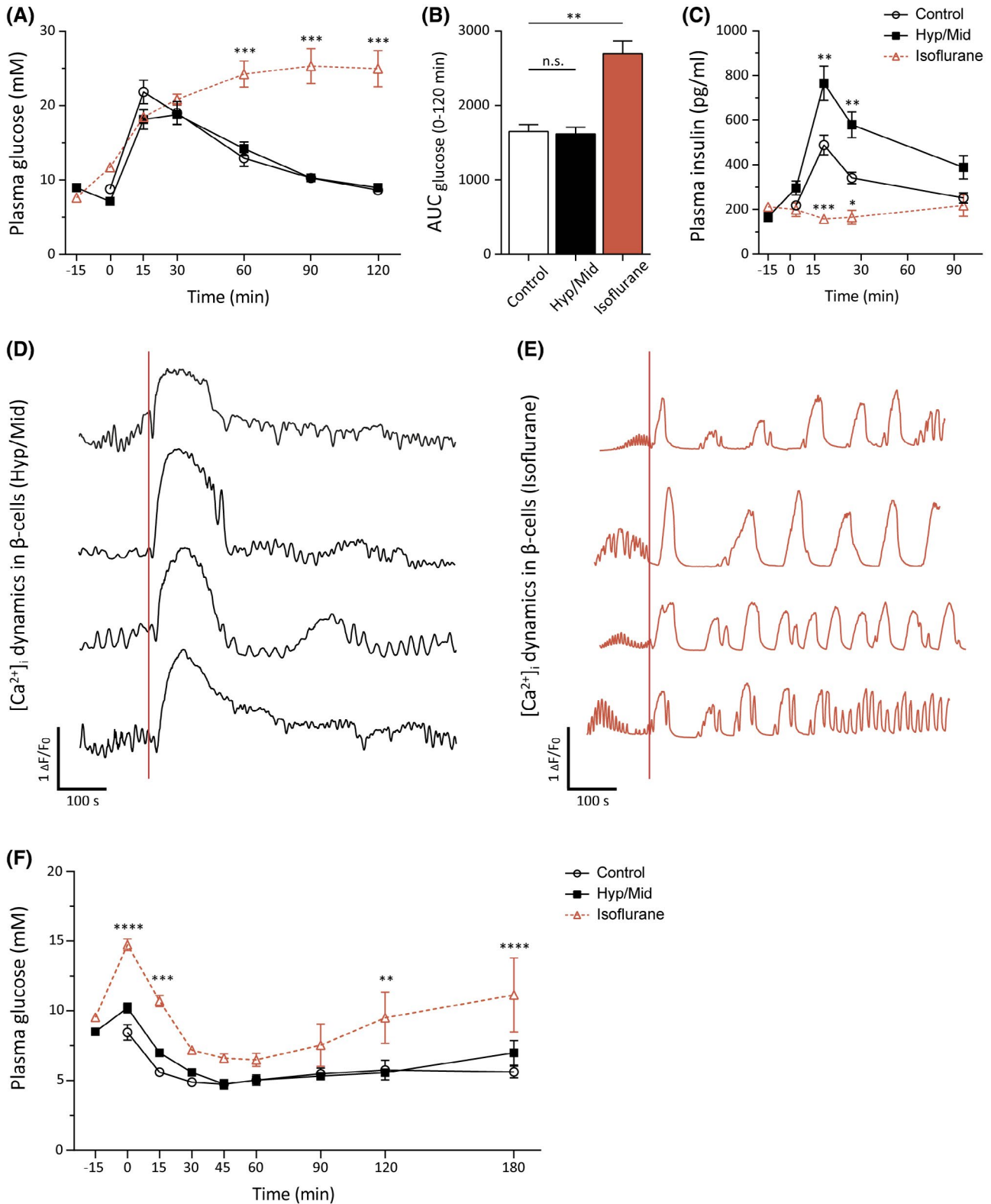


FIGURE 4 Impact of anesthetics on glucose metabolism and β -cells $[Ca^{2+}]_i$ dynamics. A, Intraperitoneal glucose tolerance test (IpGTT) in 10-weeks-old female C57Bl/6J mice that were non-anesthetized (Control) or anesthetized with either hypnorm/midazolam (Hyp/Mid) or isoflurane (Isoflurane). Plasma glucose levels were measured at the indicated time points during the IpGTT. Time point -15 minutes represents the pre-anesthetic plasma glucose levels. Time point 0 minutes displays the plasma glucose levels before glucose injection; Control $n = 8$, Hyp/Mid $n = 8$, Isoflurane $n = 7$. B, Plasma glucose data of the IpGTT were used to calculate the area under the curve (AUC) for glucose concentration between time 0 and 120 minutes. C, Illustration of the plasma insulin levels at the indicated time points during the IpGTT. D,E, Representative β -cell $[Ca^{2+}]_i$ dynamics of RIP-Cre:GCaMP3 islets transplanted into the ACE of 10-weeks-old female C57Bl/6J mice imaged after 4 hours fasting and anesthetized with either Hyp/Mid (D) or isoflurane (E) during the in vivo imaging. $[Ca^{2+}]_i$ dynamics for both groups are averaged single β -cell $[Ca^{2+}]_i$ traces expressed as a fluorescence increase (ΔF) over the basal fluorescence signal (F_0). $[Ca^{2+}]_i$ dynamics are shown before and after intravenous glucose injection (red line). F, Intraperitoneal insulin tolerance test (IpITT) of 10-weeks-old female C57Bl/6J mice that were non-anesthetized (Control) or anesthetized with either hypnorm/midazolam (Hyp/Mid) or isoflurane (Isoflurane). Plasma glucose levels were measured at the indicated time points during the IpITT. Time point -15 minutes represents the pre-anesthetic plasma glucose levels. Time point 0 minute displays the plasma glucose levels before insulin injection; Control $n = 4$, Hyp/Mid $n = 4$, Isoflurane $n = 4$. The statistical significance was estimated by two-way ANOVA with Tukey's multiple comparisons test; data are presented as means \pm SEM; * $P < .05$ ** $P < .01$, *** $P < .001$, **** $P < .0001$

noticeable $[Ca^{2+}]_i$ oscillations, the young leptin-deficient $Lep^{ob/ob}$ animals (Young Ob) exhibited a completely different $[Ca^{2+}]_i$ pattern with few $[Ca^{2+}]_i$ oscillations and lack of initial peak after glucose injection. On average, blood glucose levels measured prior to $[Ca^{2+}]_i$ imaging revealed higher concentration in mice from the Young Ob group compared to Young Lean mice (Figure 5B). In contrast, Old Lean and Old Ob mice showed lower but similar basal blood glucose levels, which is consistent with the well-characterized $Lep^{ob/ob}$ mice phenotype.¹⁸ The same tendency was observed when blood glucose levels were measured post $[Ca^{2+}]_i$ imaging, with maintained high blood glucose levels in the Young Ob mice group compared to the other groups, suggesting that the basal $[Ca^{2+}]_i$ levels in Young Ob mice are higher than in the other mouse groups based on their elevated basal glucose levels. Consequently, the hyperglycemia in Young Ob mice might lead to already stimulated β cells at the basal state, which are then incapable to respond to an additional glucose stimulus. This assumption is supported by the peak height quantification of the initial $[Ca^{2+}]_i$ peak after glucose injection, which demonstrates a drastically reduced β -cell capacity to respond to glucose in Young Ob mice compared with the other animal groups (Figure 5C). The old mice groups exhibited significantly higher first peak stimulation after glucose injection in comparison with their corresponding younger animals. This suggests that their lower basal blood glucose levels promote these islets to be more glucose responsive. To obtain more detailed data about the functional capacity of the transplanted sensor islets, we determined the percentage of β cells per islet which can respond to glucose stimulation (Figure 5D). Responding β cells were defined as single cells which increase their fluorescence intensity after the glucose challenge by at least twofold compared to the standard deviation of their basal fluorescence prior to glucose stimulation. We observed that in Young Lean mice more than $84 \pm 5\%$ (mean \pm SEM) of β cells per islet responded to glucose, while in hyperglycemic Young Ob mice the percentage of responding β cells was significantly reduced to levels around

$23 \pm 7\%$ (mean \pm SEM). These results support the view that β cells in Young Ob mice have already reached a highly stimulated status under basal conditions as a consequence of the high blood glucose levels and that only a minor percentage of β cells was still capable to respond to an additional glucose challenge. However, correlation analysis between responding β cells and the basal glucose concentration in the individual experiments shows that islets in Young Lean mice respond better to glucose than islets in Young Ob, even when selecting experiments which start at the same basal glucose concentration (Figure 5E). This suggests that islet $[Ca^{2+}]_i$ response is impaired in Young Ob mice, beyond what can be controlled solely by the basal glucose concentration. The Old mice groups presented significantly higher percentages of responding β cells in comparison with their corresponding Young mice groups. This confirms an increased sensitivity to glucose and additionally mirrors the normalization of the pathological Ob phenotype.

4 | DISCUSSION

In this study, we describe an imaging modality that allows monitoring of β -cell $[Ca^{2+}]_i$ dynamics in pancreatic islets in 3D in the living organism. We have addressed modes of image acquisition and processing as well as the choice of anesthesia. We then employed this setup to study GCaMP3-expressing sensor islets transplanted into a well-characterized diabetic mouse model.

Assessment of cell functional parameters in vivo is associated with a number of challenges. The pancreatic islets are spheroid-shaped micro-organs in which the temporal and spatial collective $[Ca^{2+}]_i$ pattern of individual β cells has been studied particularly in vitro and ex vivo revealing that β cells form an activity-dependent gap junction network consisting of locally clustered sub-compartments.^{5,19,20} Although this is clearly a three-dimensional phenomenon, the mentioned studies have monitored β -cell connectivity only within a

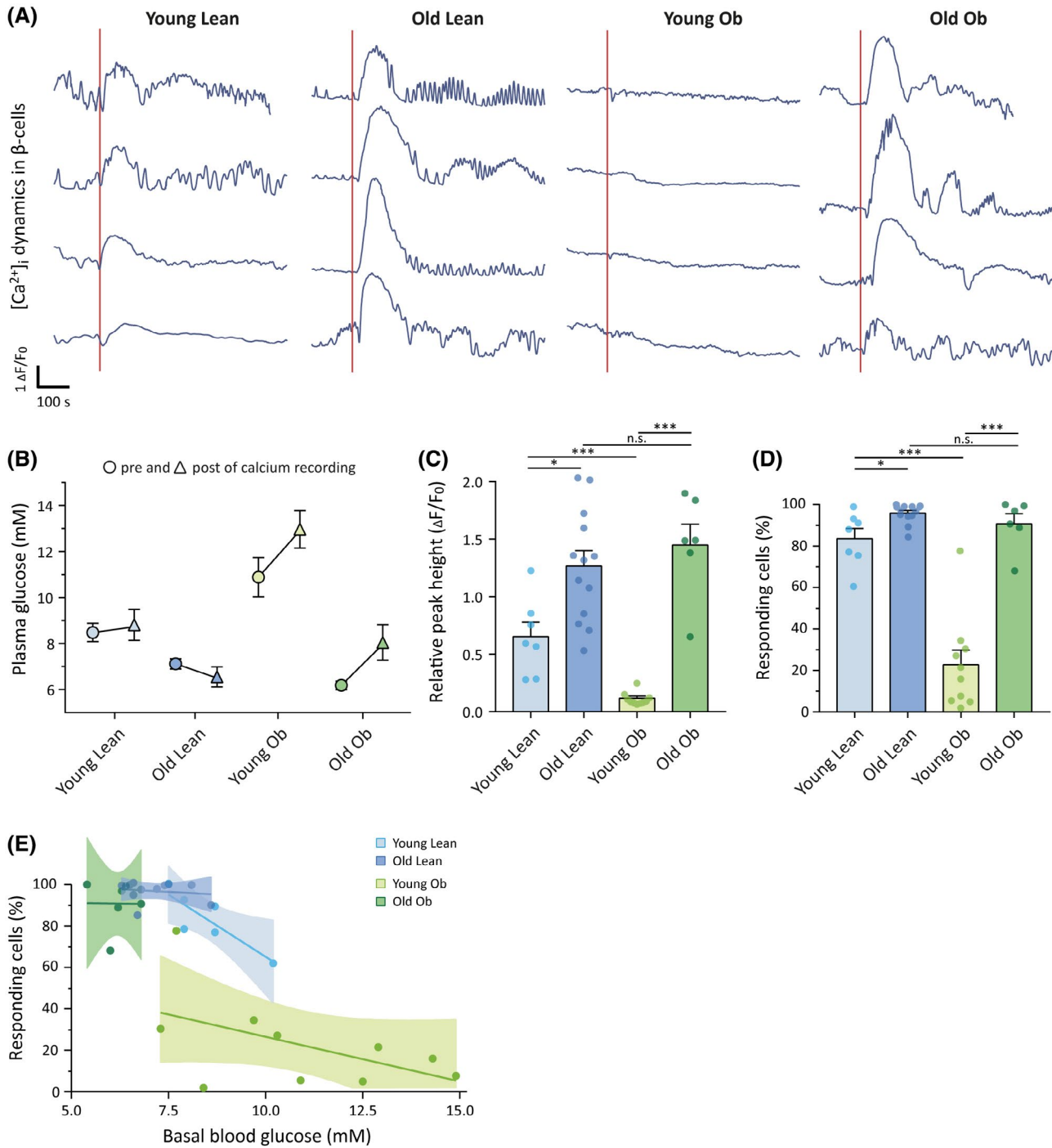


FIGURE 5 Analysis of glucose-stimulated β -cell $[Ca^{2+}]_i$ dynamics in different mouse models. A, Representative illustration of the averaged single β -cell $[Ca^{2+}]_i$ traces in response to intravenous glucose challenge indicated by the red line. RIP-Cre:GCaMP3 sensor islets were transplanted into the ACE of recipient animals 4 weeks prior to recording. Recipient animal groups were either female $Lep^{+/+}$ (Lean) or $Lep^{ob/ob}$ (Ob) mice which both were either 2 months (Young) or 10 months (Old) old at the time of islet transplantation. B, The blood glucose levels of anesthetized recipient mice were measured before (O) and after (Δ) in vivo recordings. C, The average height of the maximal $[Ca^{2+}]_i$ peak after glucose stimulation was calculated using single β -cell $[Ca^{2+}]_i$ profiles relative to their basal fluorescence intensity. Circles represent the result of one sensor islet recording in one independent experimental animal. D, Individual β cells were assessed as responding if the glucose-induced elevation of fluorescence intensity was more than twice as large as the standard deviation of the fluorescence intensity prior to glucose injection. Percentage of responding β cells is denoted per islet. Circles represent the result of one sensor islet recording in one independent experimental animal. E, Correlation between blood glucose concentration and β -cell activity. Percentage of responding cells is plotted versus basal blood glucose concentration for every individual experiment. The linear regression is shown for each of the four experimental groups together with the confidence interval with 95% confidence level. The statistical significance was estimated by nonparametric Mann-Whitney U test; data are presented as mean \pm SEM; * $P < .05$, *** $P < .001$; the sample size indicates the number of independent $[Ca^{2+}]_i$ recordings and corresponds to the number of recipient animals, Young Lean $n = 7$, Old Lean $n = 13$, Young Ob $n = 10$, Old Ob $n = 6$

single focal plane over time. Therefore, we set up an acquisition of three-dimensional information which can capture a more complex picture of the coordinated β cells and serve as a complete islet $[Ca^{2+}]_i$ pattern readout. We met the methodological challenges by reaching single-cell resolution in three dimensions as well as time resolution of 1 second for the entire volume. Photodamage has to be prevented by attenuation of the fluorescence excitation light leading to low light levels with low signal-to-noise ratio, which we improved by wavelet-based image denoising. The *in vivo* situation adds motion artifacts that have to be corrected to follow the same cell over time, which we improved by stack alignment. The high speed is achieved by widefield fluorescence detection with an EMCCD camera in combination with a fast piezo-driven z-focus. This generates a relatively low z-resolution, which we improved by stack deconvolution.

One relevant aspect for the network analysis of β cells is the modality and timing sequence of glucose exposure and $[Ca^{2+}]_i$ response. The glucose stimulation of β cells *in vitro* depends on slow diffusion of glucose into the islet interstitium causing a delay in the order of minutes until the glucose concentration reaches an equal level everywhere in the islet.¹⁷ Since islets *in situ* are exposed to glucose via blood vessel fenestration, previous *in vitro* findings may need to be interpreted in light of glucose delivery dynamics to the β cells. Due to the altered dynamics of glucose distribution, the β -cell $[Ca^{2+}]_i$ response to rising glucose concentrations might differ in terms of stimuli responsiveness, network connectivity, and functional heterogeneity comparing *in vitro* and *in vivo* measurements.

Our *in vivo* data of intraocular islet allografts show that, after the intravenous glucose injection has reached the islet vasculature, it takes only about 2 seconds until the islet interstitium is completely filled with glucose. This nearly simultaneous exposure of all β cells to blood glucose is in definite contrast to the diffusion dynamics of *in vitro* models. By inserting a glucose oxidase-based glucose micro-sensor into *in vitro* islets, it has been demonstrated that it takes up to several minutes until the glucose concentration reaches a steady state within islets in culture.²¹ Our 2-NBDG data show that small molecules like glucose rapidly leave the islet vasculature and diffuse evenly across the interstitial space of the islet. This fast 2-NBDG propagation in vascularized islets has also been observed in *in situ* experiments directly in the pancreas,²² suggesting that the eye transplantation site is similar to the physiological situation in terms of glucose exposure. Furthermore, we could demonstrate that the coupling of glucose stimulus to $[Ca^{2+}]_i$ response in β cells takes only 12 ± 1 (mean \pm SEM) seconds *in vivo*. In contrast, the glucose stimulus depending on diffusion causes a significant time delay of the β -cell $[Ca^{2+}]_i$ response, which was increased from the outer layer toward the center of a non-vascularized islet *in vitro*. Although this altered response modality primarily

plays a role for the initial phase of the β -cell $[Ca^{2+}]_i$ response and could be affected by dissimilar basal glucose concentration, it highlights an important difference between the experimental setup *in vitro* and *in vivo*. The shortened glucose response time in our *in vivo* imaging setup is likely related to the intravenous glucose administration and vascularization and emphasizes that proper physiological conditions are vital for the precise interpretation of β -cell $[Ca^{2+}]_i$ responses.

It has been known for decades that volatile anesthetics such as isoflurane can impair insulin secretion and glucose homeostasis,²³ which is also the case in humans.²⁴ However, the precise mechanism is still controversial. Since we require anesthesia for the non-invasive *in vivo* imaging, we conducted a comparative study using either isoflurane or Hyp/Mid (mixture of fentanyl-fluanisone-midazolam) to determine side effects on glucose-induced $[Ca^{2+}]_i$ response in β cells. In the glucose tolerance tests, we could confirm that insulin secretion is hampered in mice anesthetized with isoflurane due to continuously increased blood glucose levels. Although the secretory function of β cells is disrupted, we could detect a uniform and continuous $[Ca^{2+}]_i$ oscillation pattern after glucose stimulation. This $[Ca^{2+}]_i$ profile differs from that obtained using Hyp/Mid, but still suggests that neither the glucose-sensing mechanism nor the initiation of Ca^{2+} influx is severely compromised in β cells during isoflurane anesthesia. This observation is in contrast to previous studies where the isoflurane-induced inhibition of secretory vesicle undergoing exocytosis has been linked to either ATP-sensitive K^+ channels or voltage-gated Ca^{2+} channels.^{25,26} However, our results rather indicate that isoflurane affects the secretory function of β cells by uncoupling Ca^{2+} signaling from vesicle exocytosis. It may be speculated that administration of lipophilic anesthetics such as isoflurane can lead to lipid bilayer disorganization causing a disruption of the vesicle docking mechanism in β cells. This is supported by previous studies which have shown that, on the one hand, isoflurane can influence the compactness and lateral organization of lipid bilayers,²⁷ and on the other hand, that a lipid-induced dissociation of Ca^{2+} channels from secretory vesicles can prevent insulin secretion.²⁸ Since β -cell $[Ca^{2+}]_i$ oscillations are dissociated from the endocrine function under isoflurane anesthesia, this compound is not appropriate for our *in vivo* imaging experiments. The observation that β cell $[Ca^{2+}]_i$ can be uncoupled from insulin secretion has already been described in earlier studies.²⁹ Nevertheless, a recent study, which characterized in great detail Ca^{2+} handling of the β -cell network *in vivo*, used isoflurane for animal anesthesia and thereby left an open question whether the islet physiology was affected.³⁰

In our study, on the contrary, animals anesthetized with Hyp/Mid reveal a blood glucose homeostasis similar to non-anesthetized control animals during GTT tests, except for a noticeable increase in blood insulin levels. However, we could demonstrate that the higher insulin levels observed

in animals with Hyp/Mid anesthesia is caused neither by peripheral insulin resistance nor by a direct enhancement of insulin exocytosis in the β cell. Since integration of other physiological factors could play a role for the endocrine function of β cells in vivo, one might speculate whether the Hyp/Mid anesthesia affects the innervation or the endocrine-exocrine communication of the pancreatic islets. It has been demonstrated in previous experiments that intraocular-transplanted islets are innervated by the rich parasympathetic and sympathetic nervous supply of the iris and that the nervous input was capable to manipulate the metabolic function of the innervated islet leading to reduced fasting glycemia and improved glucose tolerance.⁷ Since anesthesia primarily affects the nervous system, we cannot exclude such an influence in our study, but cannot determine it either due to the lack of an appropriate in vivo model without anesthesia. Although Hyp/Mid is as lipophilic as isoflurane, our in vitro experiments suggest that both insulin secretion and $[Ca^{2+}]_i$ handling of β cells are not impaired by this anesthetic agent. Previous studies have shown that the glucose metabolism of mice anesthetized with the same fentanyl-fluanisone combination remains unaltered, if the animals were fasted before anesthesia.³¹ In summary, Hyp/Mid seems to be a suitable anesthetic for measuring glucose-dependent $[Ca^{2+}]_i$ dynamics in pancreatic β cells, although we ultimately lack the comparison to β -cell $[Ca^{2+}]_i$ dynamics in non-anesthetized animals.

Transplantation of GCaMP3-expressing sensor islets into the ACE of mice of four different animal groups enabled us to explore differences within the β -cell $[Ca^{2+}]_i$ dynamics in response to glucose stimulation. We could demonstrate that almost all β cells respond to a glucose challenge in healthy animals with normoglycemia, whereas in hyperinsulinemic/hyperglycemic Young Ob mice $[Ca^{2+}]_i$ appears to be highly stimulated. The response pattern of β -cell $[Ca^{2+}]_i$ to glucose stimulation in healthy mice corresponds to the response pattern obtained from in vitro studies, except for several distinct differences. Similar to in vitro recordings, the glucose stimulation in vivo led to a rapid increase in β -cell $[Ca^{2+}]_i$ followed by slow and fast $[Ca^{2+}]_i$ oscillations.³² In contrast to most in vitro studies, the intraocular islets were already stimulated under basal conditions due to the physiologically higher resting blood glucose levels of the animals compared to 3 mM glucose concentration used as basal status in vitro. This fact could also explain the aforementioned fast β -cell $[Ca^{2+}]_i$ response to the injected glucose. β cells in vivo seem to be ready to respond immediately, whereas β cells in vitro starved at 3 mM glucose require a prolonged period of time to respond. In this context, the individual animal-dependent variation of basal blood glucose levels seem to be an influential confounder. Many more animals per group would be needed to rule this out, which would go beyond the present

study. One important characteristic of synchronized β -cell $[Ca^{2+}]_i$ dynamics is the existence of fast $[Ca^{2+}]_i$ oscillations. While we have been able to identify fast $[Ca^{2+}]_i$ oscillations in the three healthy control groups, we could not see any fast oscillations in the Young Ob mice, which is in contrast to existing in vitro studies.³³ In healthy animals, the majority of β cells participated in fast $[Ca^{2+}]_i$ oscillations, which occurred every 10–20 seconds, similar to in vitro studies.²⁰ Although the majority of β cells seem to be constantly stimulated in the high blood glucose milieu of Young Ob mice, about 20% of β cells can still respond to an additional glucose challenge. Thereby, we clearly identify two β -cell populations which differ in their glucose sensitivity and responsiveness. This β -cell heterogeneity might be based upon functional adaptation that has developed during the permanent exposure to elevated blood glucose levels in Young Ob mice. Such adaptation may in addition explain why the percentage of responding cells differs between Young Ob and Young Lean mice even if comparing experiments with equal basal blood glucose values. Technically, the percentage of responding cells is a good example of an important parameter that can be calculated based on single-cell data from our imaging setup.

In summary, we have introduced an instrumental imaging platform to analyze in vivo pancreatic β -cell $[Ca^{2+}]_i$ response patterns at single-cell resolution in health and disease. We could demonstrate that the dynamics of glucose exposure to β cells in vivo is different from the dynamics in vitro due to intra-islet blood circulation. Moreover, we have critically evaluated the choice of an appropriate anesthetic agent showing that it is crucial for the in vivo imaging to avoid impact on glucose metabolism and Ca^{2+} signaling. Finally, by examining the single β -cell $[Ca^{2+}]_i$ response patterns of sensor islets engrafted into different metabolic milieus, we observed a sustained adaptation of β -cell function indicating functional heterogeneity of β cells in vivo. Through the combination of intraocular-transplanted Ca^{2+} -reporting islets and the imaging technology presented here, we now have the possibility to dissect the pancreatic β -cell network in vivo with respect to questions like connectivity, synchronization, and functional heterogeneity while putting the knowledge gained from previous in vitro investigations to test.

ACKNOWLEDGMENTS

This work was supported by funds from the Swedish Research Council, the Family Erling-Persson Foundation, the Novo Nordisk Foundation, the Stichting af Jochnick Foundation, the Swedish Diabetes Association, the Scandia Insurance Company Ltd., Diabetes Research and Wellness Foundation, Berth von Kantzow's Foundation, the Strategic Research Program in Diabetes at Karolinska Institutet, the ERC-2013-AdG 338936 BETAIMAGE, the ERC-2017-PoC

727306 BETASCREEN, the ERC-2018-AdG 834860 EYELETS, the Swedish Foundation for Strategic Research, and the Knut and Alice Wallenberg Foundation. P.-OB and SJ are the guarantors of this work. MV was supported by a Novo Nordisk post-doctoral fellowship run in partnership with Karolinska Institutet. Finally, we would like to thank Hamamatsu Photonics, Sweden, for their technical support.

CONFLICT OF INTEREST

During the course of this work, SJ was employed by Biocrine AB, holding the patents of the transplantation method. BL, MK, and IL are consultants to Biocrine AB and P.-OB is CEO of Biocrine AB.

AUTHOR CONTRIBUTIONS

P.-O. Berggren was the originator of this project; S. Jacob, M. Köhler, P. Tröster, I. B. Leibiger, and P.-O. Berggren designed the experimental strategy; S. Jacob, M. Visa, C.F. García-Prieto, T. Alanentalo, T. Moede, and B. Leibiger performed the experimental work; S. Jacob contributed new analysis methods and wrote the original draft of the article; S. Jacob, M. Köhler, P. Tröster, and M. Visa analyzed data; P. Tröster wrote the final version of the article, which was critically reviewed and edited by M. Köhler, M. Visa, I. B. Leibiger, and P.-O. Berggren; I. B. Leibiger and P.-O. Berggren supervised the project and acquired funding.

REFERENCES

- Röder PV, Wu B, Liu Y, Han W. Pancreatic regulation of glucose homeostasis. *Exp Mol Med*. 2016;48:e219.
- Satin LS. Localized calcium influx in pancreatic β -cells: its significance for Ca^{2+} -dependent insulin secretion from the islets of Langerhans. *Endocrine*. 2000;13:251-262.
- Rorsman P, Braun M, Zhang Q. Regulation of calcium in pancreatic α - and β -cells in health and disease. *Cell Calcium*. 2012;51:300-308.
- Stožer A, Dolenšek J, Rupnik MS. Glucose-stimulated calcium dynamics in islets of Langerhans in acute mouse pancreas tissue slices. *PLoS One*. 2013;8:e54638.
- Johnston NR, Mitchell RK, Haythorne E, et al. Beta cell hubs dictate pancreatic islet responses to glucose. *Cell Metab*. 2016;24:389-401.
- Westacott MJ, Ludin NWF, Benninger RKP. Spatially organized β -cell subpopulations control electrical dynamics across islets of Langerhans. *Biophys J*. 2017;113:1093-1108.
- Rodríguez-Díaz R, Speier S, Damaris R, et al. Noninvasive in vivo model demonstrating the effects of autonomic innervation on pancreatic islet function. *Proc Natl Acad Sci USA*. 2012;109:21456-21461.
- Speier S, Nyqvist D, Leibiger IB, et al. Noninvasive in vivo imaging of pancreatic islet cell biology. *Nat Med*. 2008;14:574-578.
- Chen C, Chmelova H, Cohrs CM, et al. Alterations in β -cell calcium dynamics and efficacy outweigh islet mass adaptation in compensation of insulin resistance and prediabetes onset. *Diabetes*. 2016;65:2676-2685.
- Speier S, Nyqvist D, Köhler M, Caicedo A, Leibiger IB, Berggren P-O. Noninvasive high-resolution in vivo imaging of cell biology in the anterior chamber of the mouse eye. *Nat Protoc*. 2008;3:1278-1286.
- Boutet de Monvel J, Le Calvez S, Ulfendahl M. Image restoration for confocal microscopy: improving the limits of deconvolution, with application to the visualization of the mammalian hearing organ. *Biophys J*. 2001;80:2455-2470.
- Guizar-Sicairos M, Thurman ST, Fienup JR. Efficient subpixel image registration algorithms manual. *Opt Lett*. 2008;33:156-158.
- Zanella R, Zanghirati G, Cavicchioli R, et al. Towards real-time image deconvolution: application to confocal and STED microscopy. *Sci Rep*. 2013;3:2523.
- Kroon DJ. *Segmentation of the Mandibular Canal in Cone-Beam CT Data*. Enschede, Netherlands: University of Twente; 2011.
- Rutter GA, Hodson DJ, Chabosseau P, Haythorne E, Pullen TJ, Leclerc I. Local and regional control of calcium dynamics in the pancreatic islet. *Diabetes Obes Metab*. 2017;19:30-41.
- Ilegems E, Dicker A, Speier S, et al. Reporter islets in the eye reveal the plasticity of the endocrine pancreas. *Proc Natl Acad Sci*. 2013;110:20581-20586.
- Bertram R, Parnarowski M. Glucose diffusion in pancreatic islets of Langerhans. *Biophys J*. 1998;74:1722-1731.
- Lindström P. The physiology of obese-hyperglycemic mice [ob/ob mice]. *Sci World J*. 2007;7:666-685.
- Stožer A, Gosak M, Dolenšek J, et al. Functional connectivity in islets of Langerhans from mouse pancreas tissue slices. *PLoS Comput Biol*. 2013;9:1-12.
- Benninger RKP, Zhang M, Steven Head W, Satin LS, Piston DW. Gap junction coupling and calcium waves in the pancreatic islet. *Biophys J*. 2008;95:5048-5061.
- Kauri LM, Jung SK, Kennedy RT. Direct measurement of glucose gradients and mass transport within islets of Langerhans. *Biochem Biophys Res Commun*. 2003;304:371-377.
- Michau A, Hodson DJ, Fontanaud P, et al. Metabolism regulates exposure of pancreatic islets to circulating molecules in vivo. *Diabetes*. 2016;65:463-475.
- Desborough JP, Jones PM, Howell SL, Landon MJ, Persaud SJ. Isoflurane inhibits insulin secretion from isolated rat pancreatic islets of Langerhans. *Br J Anaesth*. 1993;71:873-876.
- Behdad S, Mortazavizadeh A, Ayatollahi V, Khadiv Z, Khalilzadeh S. The effects of propofol and isoflurane on blood glucose during abdominal hysterectomy in diabetic patients. *Diabetes Metab J*. 2014;38:311-316.
- Tanaka K, Kawano T, Nakaya Y, et al. Mechanisms of impaired glucose tolerance and insulin secretion during isoflurane anesthesia. *Anesthesiology*. 2009;111:1044-1051.
- Torturo CL, Zhou Z-Y, Ryan TA, Hemmings HC. Isoflurane inhibits dopaminergic synaptic vesicle exocytosis coupled to $\text{Ca}_v2.1$ and $\text{Ca}_v2.2$ in rat midbrain neurons. *Eneuro*. 2019;6:1-13.
- Turkyilmaz S, Almeida P, Regen S. Effects of isoflurane, halothane and chloroform on the interactions and lateral organization of lipids in the liquid-ordered phase. *Langmuir*. 2011;27:14380-14385.
- Hoppa MB, Collins S, Ramracheya R, et al. Chronic palmitate exposure inhibits insulin secretion by dissociation of Ca^{2+} channels from secretory granules. *Cell Metab*. 2009;10:455-465.
- Berggren PO, Arkhammar P, Zaitsev SV, Efendic S, Bertorello AM. Dissociation between changes in cytoplasmic free Ca^{2+} concentration

- and insulin secretion as evidenced from measurements in mouse single pancreatic islets. *Proc Natl Acad Sci*. 1995;92:9712-9716.
30. Salem V, Silva LD, Suba K, et al. Leader β -cells coordinate Ca^{2+} dynamics across pancreatic islets in vivo. *Nat Metab*. 2019;1:615-629.
 31. Johansen O, Vaaler S, Jorde R, Reikerås O. Increased plasma glucose levels after Hypnorm® anaesthesia, but not after Pentobarbital® anaesthesia in rats. *Lab Anim*. 1994;28:244-248.
 32. Valdeolmillos M, Soria B, Rosario LM, Santos RM, Contreras D. Glucose-induced oscillations of intracellular Ca^{2+} concentration resembling bursting electrical activity in single mouse islets of Langerhans. *FEBS Lett*. 1989;259:19-23.
 33. Irles E, Quesada I, Carneiro EM, et al. Enhanced glucose-induced intracellular signaling promotes insulin hypersecretion: pancreatic

beta-cell functional adaptations in a model of genetic obesity and prediabetes. *Mol Cell Endocrinol*. 2015;404:46-55.

SUPPORTING INFORMATION

Additional supporting information may be found online in the Supporting Information section.

How to cite this article: Jacob S, Köhler M, Tröster P, et al. In vivo Ca^{2+} dynamics in single pancreatic β cells. *The FASEB Journal*. 2020;34:945–959. <https://doi.org/10.1096/fj.201901302RR>